

Research Paper

Molecular imaging of T cell co-regulator factor B7-H3 with ^{89}Zr -DS-5573a

Ingrid Julienne Georgette Burvenich^{1,2*}, Sagun Parakh^{1,2,3*}, Fook-Thean Lee¹, Nancy Guo¹, Zhanqi Liu^{1,2}, Hui Kong Gan^{1,2,3,4}, Angela Rigopoulos^{1,2}, Graeme Joseph O'Keefe^{4,5}, Sylvia Jie Gong^{5,6}, Yit Wooi Goh¹, Henri Tochon-Danguy⁵, Fiona Elizabeth Scott^{1,2}, Masakatsu Kotsuma⁷, Kenji Hirotsani⁸, Giorgio Senaldi⁹ and Andrew Mark Scott^{1,2,3,4,5}✉

1. Tumour Targeting Laboratory, Ludwig Institute for Cancer Research and Olivia Newton-John Cancer Research Institute, Melbourne, Australia
2. School of Cancer Medicine, La Trobe University, Melbourne, Australia
3. Department of Medical Oncology, Austin Health, Heidelberg, Melbourne, Australia
4. Department of Medicine, University of Melbourne, Melbourne, Australia
5. Department of Molecular Imaging and Therapy, Austin Health, Melbourne, Australia
6. School of Engineering and Mathematical Sciences, La Trobe University
7. Quantitative Clinical Pharmacology & Translational Sciences, Daiichi Sankyo, Inc., Basking Ridge, NJ, USA
8. Biologics & Immuno-Oncology Laboratories, Daiichi-Sankyo Co., Ltd., Tokyo, Japan
9. Department of Translational Medicine and Clinical Pharmacology, Daiichi-Sankyo Pharma Development, Edison, NJ, USA

* - authors contributed equally

✉ Corresponding author: Professor Andrew M. Scott, Tumour Targeting Laboratory, Olivia Newton-John Cancer Research Institute, Level 5, ONJ Cancer Centre, 145 Studley Road, Heidelberg, Victoria 3084, Australia. Phone: 61-39496-5876; Fax: 61-39496-5334; E-mail: andrew.scott@onjcri.org.au

© Ivyspring International Publisher. This is an open access article distributed under the terms of the Creative Commons Attribution (CC BY-NC) license (<https://creativecommons.org/licenses/by-nc/4.0/>). See <http://ivyspring.com/terms> for full terms and conditions.

Received: 2018.02.15; Accepted: 2018.06.12; Published: 2018.07.30

Abstract

B7-H3 is a transmembrane protein widely expressed in a variety of cancers and has been shown to play a role in anti-tumor immunity. This study aims to develop a molecular imaging probe to identify B7-H3 expression in tumors and to develop ^{89}Zr -DS-5573a as a theranostic that could aid patient selection in clinical Phase I studies.

Methods: The anti-B7-H3 humanised monoclonal antibody DS-5573a was labeled with zirconium-89 (^{89}Zr -), and assessed for radiochemical purity, immunoreactivity (Lindmo analysis), antigen binding affinity (Scatchard analysis), and serum stability *in vitro*. *In vivo* biodistribution and imaging studies were performed with positron emission tomography and magnetic resonance imaging (PET/MRI) studies to identify and quantitate ^{89}Zr -DS-5573a tumor uptake in a B7-H3-positive breast cancer model (MDA-MB-231) and a B7-H3-negative murine colon cancer model (CT26). Imaging and biodistribution studies were also performed in MDA-MB-231 tumor-bearing SCID mice in the absence and presence of therapeutic DS-5573a antibody dose (3 mg/kg DS-5573a).

Results: ^{89}Zr -DS-5573a showed high and specific binding to B7-H3-expressing MDA-MB-231 cells (immunoreactivity on day 0, $75.0 \pm 2.9\%$), and low binding to B7-H3-negative CT26 cells (immunoreactivity on day 0, $10.85 \pm 0.11\%$) *in vitro*. ^{89}Zr -DS-5573a demonstrated good serum stability *in vitro* with $57.2 \pm 2.0\%$ of immunoreactivity remaining on day 7. *In vivo* biodistribution studies showed high uptake of ^{89}Zr -DS-5573a in B7-H3-expressing MDA-MB-231 tumor-bearing mice, achieving $32.32 \pm 6.55\%$ ID/g on day 7 post injection in BALB/c *nu/nu* mice and $25.76 \pm 1.79\%$ ID/g in SCID mice, with minimal evidence of non-specific uptake in normal tissues, and excellent tumor localization on PET/MRI. In a combined imaging/therapy study, receptor saturation was demonstrated in tumors responding to therapy.

Conclusion: ^{89}Zr -DS-5573a demonstrates specific and prolonged targeting of B7-H3-expressing tumors *in vivo*. Saturation of binding sites was demonstrated in tumors responding to DS-5573a therapy. These results indicate that ^{89}Zr -DS-5573a has potential to target B7-H3-expressing tumors in cancer patients. Furthermore ^{89}Zr -DS-5573a has the potential to provide important insights into T cell biology through its specific binding to B7-H3.

Key words: PET, DS-5573a, B7-H3, zirconium-89, immunotherapy

Introduction

T cell activation requires two signals; the first occurs through the engagement of the T cell receptor by the major histocompatibility complex on antigen-presenting cells. The second signal is antigen independent and occurs through the engagement of the B7/CD28 family of co-stimulatory molecules. The B7 family comprises seven members and can be divided into three groups based on phylogenetic analysis: group I (B7-1, B7-2, and B7h), group II (PD-L1 and PD-L2) and group III (B7x and B7-H3) [1]. Immunomodulatory drugs targeting members of the B7 family, such as PD-L1, have shown impressive response rates in a variety of tumor types in early phase clinical trials [2-7].

Human B7-H3 (B7 homolog 3 or CD276) is a type 1 transmembrane protein that has its extracellular region encoded by duplicated V-like and C-like immunoglobulin domains [8]. B7-H3 has a co-stimulatory role through T cell proliferation and interferon- γ induction [9]. Interestingly, B7-H3 has also been shown to inhibit T cell-dependent responses in B7-H3-deficient mice and inhibit natural killer cell cytotoxic function, by binding to an inhibitory receptor [10-12]. B7-H3 protein is not constitutively expressed on immune cells, but its expression can be induced in T cells, natural killer (NK) cells, and antigen-presenting cells [13]. Although B7-H3 mRNA has been reported in various normal tissues [9], B7-H3 protein expression is more limited [14-16]. In contrast, B7-H3 overexpression has been reported in a variety of cancers including breast [17, 18], prostate [19, 20], ovarian [21], renal cell [22], colorectal [23] and urothelial cancers [24]. B7-H3 expression is significantly higher on tumor vascular endothelial cells as compared to normal tissue [17, 20, 25]. In some cancer types, B7-H3 overexpression is associated with an aggressive cancer phenotype [26, 27] resulting in an increase in risk of cancer recurrence, cancer metastases and poorer patient outcome [1, 28-30]. Preclinical studies have shown that siRNA knockdown of B7-H3 expression reduces cell adhesion, migration, and invasion in melanoma, breast and prostate cancer cells [26, 27].

Preclinical studies with contrast-enhanced ultrasound imaging using microbubbles have shown the potential in identifying cancerous lesions early in preclinical models by targeting B7-H3 on endothelial cells [17]. DS-5573a is an anti-human B7-H3 afucosylated humanized antibody generated by Daiichi Sankyo [31]. DS-5573a induces high antibody-dependent cellular cytotoxicity *in vitro* against cell lines ranging from low (COLO205, 1.7×10^4 receptors/cell) to high (NCI-H322, 3.4×10^5 receptors/cell) B7-H3 expression. *In vivo*,

dose-dependent anti-tumor activity of DS-5573a was demonstrated in MDA-MB-231-bearing SCID mice with significant tumor growth inhibition observed at doses as low as 0.03 mg/kg [31]. This study aimed to develop a molecular imaging probe to B7-H3, through desferrioxamine chelation and ^{89}Zr -radiolabeling of DS-5573a, as well as characterizing the *in vitro* and *in vivo* binding properties of the radioconjugate. In addition to tracer development, combined imaging and therapy studies *in vivo* were performed to demonstrate the theranostic potential of DS-5573a, i.e., to characterize the diagnostic properties of ^{89}Zr -Df-Bz-NCS-DS-5573a in combination with treatment of the DS-5573a antibody itself.

Methods

Cell culture

The human B7-H3 antigen-expressing breast cancer cell line MDA-MB-231 and negative control murine colon cancer cell line CT26 were obtained from the American Type Culture Collection (ATCC, Manassas, MD, USA). The cells were cultured in RPMI 1640 medium (Invitrogen, Carlsbad, CA, USA) or Dulbecco modified Eagle medium respectively, with 10% foetal calf serum, 2 mM GlutaMAX (Gibco), and 100 units/mL of penicillin and 100 $\mu\text{g}/\text{mL}$ of streptomycin in a 10 mM citrate buffer (Gibco), incubated at 37 °C with 5% CO_2 .

Animal model

Cells (MDA-MB-231, 20×10^6 cells; CT26, 2×10^6 cells) were injected subcutaneously in the right flank of 5-6-week-old female BALB/c *nu/nu* mice or SCID mice (Animal Research Centre, WA, Australia). All animal studies were approved by the Austin Hospital Animal Ethics Committee and were conducted in compliance with the Australian Code for the care and use of animals for scientific purposes.

Binding activity of DS-5573a by ELISA

Recombinant murine B7-H3 (Val29-Phe244) and human B7-H3 (Leu29-Pro245) with a C-terminal 10-His tag were obtained from R&D Systems. DS-5573, a full-sized anti-human B7-H3 afucosylated humanized antibody (150 kDa) was obtained from Daiichi Sankyo. Phosphate-buffered saline (PBS) was added for reconstitution to a final concentration of 100 $\mu\text{g}/\text{mL}$. B7-H3 antigens (3 $\mu\text{g}/\text{mL}$ in PBS; 50 μL per well) were coated to 96-well maxisorp plates (Nunc) overnight at 4 °C. Plates were blocked with 3% fetal calf serum in PBS (240 $\mu\text{L}/\text{well}$) for 1 h at room temperature. A serial dilution of DS-5573a or an IgG isotype control antibody (10 $\mu\text{g}/\text{mL}$ to 3.15 ng/mL) were added to the plate in duplicate and incubated for 1 h at room temperature. Plates were washed three

times with washing buffer (0.05% Tween in PBS). Secondary goat anti-human Ig Fc-horse radish peroxidase-conjugated antibody (100 μ L per well) was added at a 1 in 2000 dilution and incubated for 1 h at room temperature. After washing three times with washing buffer, 3,3',5,5'-Tetramethylbenzidine (TMB) Liquid Substrate (Sigma) (100 μ L/well) was added and allowed to react for 10 min at room temperature before adding stop solution (2 M H₂SO₄, 50 μ L/well). Absorbance was read using an ELISA plate reader at 450 nm.

Chelation and radiolabeling of ⁸⁹Zr-labeled DS-5573a

Analytical grade reagents, sterile technique and pyrogen-free plasticware were used in all labeling steps. DS-5573a was chelated with the bifunctional metal ion chelator *p*-isothiocyanatobenzyl-desferrioxamine (Df-Bz-NCS; Macrocyclics Inc Dallas, TX, USA) at a 3.0-fold molar excess as described before [32]. Df-Bz-NCS-DS-5573a conjugates prepared in 50 mM sodium acetate buffer (BDH/VWR Chemicals, Australia), pH 5.6, containing 5% w/v sorbitol (BDH/VWR Chemicals, Australia) and 0.01% w/v Tween 80 (Croda, Australia), were aliquoted in 1.0 mg aliquots and stored at -80 °C until required.

Following chelation, DS-5573a was trace radiolabeled as follows: a solution containing 99.9 \pm 16.1 MBq (2.7 mCi) of positron-emitting ⁸⁹Zr (PerkinElmer, Melbourne, Australia) was mixed with 1.0 mg Df-Bz-NCS-DS-5573a for 45 min. The mixture was then quenched with EDTA. The product was purified on a Sephadex G50 column (Pharmacia, Uppsala, Sweden) equilibrated with sodium chloride BP, with resultant radioconjugates assessed for radiochemical purity and immunoreactivity.

Quality control and *in vitro* characterization of ⁸⁹Zr-labeled DS-5573a

Radiochemical purity was estimated by instant thin-layer chromatography (ITLC) using silica gel impregnated glass fiber ITLC strips (Gelman Sciences, Inc., An Arbor, MI, USA) and 20 mM citric acid, pH 4.8 as mobile phase. The immunoreactive fraction of the radiolabeled DS-5573a constructs with antigen-positive MDA-MB-231 cells was determined by linear extrapolation to binding at infinite antigen excess using a Lindmo assay [33] as previously described [34]. For this antibody-antigen system, 40 million cells were used in the binding assays under conditions of antigen excess. Scatchard analysis was used to calculate the apparent association constant (K_a) and number of antibody molecules bound per cell [33].

Serum stability was assessed by incubating 20 μ g ⁸⁹Zr-Df-Bz-NCS-DS-5573a in 100 μ L of human serum at 37 °C for a 7-day period. Radiochemical purity and single-point immunoreactivity assays at 0 (day of radiolabeling, no incubation), 3 and 7 days of incubation were performed with B7-H3-expressing MDA-MB-231 cells (40 \times 10⁶) under conditions of antigen excess. Single point immunoreactivity assays were also performed with the B7-H3-negative cell line CT26 on day 0. Radioconstruct integrity was assessed by size exclusion chromatography (SEC) performed on a Superdex 200HR 10/30 column (GE Healthcare) at a flow rate of 0.14 mL/min and fraction size of 3.6 mL. The elution buffer was phosphate-buffered saline at pH 7.4.

Biodistribution study with ⁸⁹Zr-labeled DS-5573a

BALB/*c nu/nu* or SCID mice with established MDA-MB-231 or CT26 tumors received a trace dose of 0.37 MBq ⁸⁹Zr-Df-Bz-NCS-DS-5573a (5 μ g, 10.1 μ Ci), intravenously via the tail vein (0.1 mL). On day 0 (2 h), 1, 2, 3, 5, and 7 after injection, groups of MDA-MB-231 tumor-bearing BALB/*c nu/nu* mice (*n* = 5) were sacrificed by overinhalation of isofluorane anaesthesia and biodistribution of radiolabeled DS-5573a in normal organs and tumors was assessed. Biodistribution studies in MDA-MB-231 tumor-bearing SCID mice (*n* = 3) and CT26 tumor-bearing SCID mice (*n* = 3) were performed on day 3 or day 7 after injection only.

At the designated time points, the mice were humanely sacrificed by isofluorane overinhalation, exsanguinated by cardiac puncture, and tumors and organs were collected immediately. All samples were counted in a dual-channel γ -scintillation counter (Wizard; PerkinElmer). Triplicate standards prepared from the injected material were counted at each time point with tissue and tumor samples, enabling calculations to be corrected for physical decay of the isotope. The tissue distribution data were calculated as the mean \pm SD percentage injected dose per gram tissue (%ID/g) for the radiolabeled construct per time point.

Molecular imaging of B7-H3

In vivo PET imaging of ⁸⁹Zr-labeled DS-5573a was performed on a separate group of three MDA-MB-231 tumor-bearing BALB/*c nu/nu* mice receiving a dose of 2.46 MBq ⁸⁹Zr-Df-Bz-NCS-DS-5573a (30 μ g, 66.5 μ Ci). Mice were imaged with positron emission tomography (PET) and magnetic resonance (MR) on day 7 post injection with a small animal camera (nanoScan® PET/MR camera, Mediso, Budapest, Hungary).

⁸⁹Zr-DS-5573a imaging in DS-5573a-treated MDA-MB-231 tumor-bearing SCID mice

To investigate the use of ⁸⁹Zr-DS-5573a as a theranostic, ⁸⁹Zr-DS-5573a PET/MR imaging was performed in DS-5573a-treated mice. MDA-MB-231 tumor-bearing SCID mice with established tumors ($83.37 \pm 13.13 \text{ mm}^3$, $n = 12$) were randomized in two groups of six mice. One group received weekly intravenous injection of DS-5573a (3 mg/kg) and the second group received vehicle control (phosphate-buffered saline, pH 7.4). After four weeks of treatment, groups of three treated and untreated mice were injected with $5 \mu\text{g}$ ⁸⁹Zr-DS-5573a ($13.3 \mu\text{Ci}$) with or without the addition of $70 \mu\text{g}$ of unlabeled DS-5573 (3 mg/kg). PET/MR imaging was performed on day 3 and day 7 post injection. After the final scan, mice were humanely sacrificed and organs were collected and radioactivity was counted in a dual-channel γ -scintillation counter. At the end of therapy (day 35), percentage tumor growth inhibition (%TGI) was calculated as follows: $\%TGI = [1 - (T/T_0 / C/C_0) / 1 - (C_0/C)] \times 100$, where T = mean tumor volume of treated at endpoint, T_0 = mean tumor volume of treated at time 0, C = mean tumor volume of control at endpoint and C_0 = mean tumor volume of vehicle control at time 0.

At the start of therapy, a separate group of six MDA-MB-231 tumor-bearing SCID mice with average tumor size of $81.91 \pm 20.66 \text{ mm}^3$ were injected

with $5 \mu\text{g}$ ⁸⁹Zr-DS-5573a ($20 \mu\text{Ci}$). Three out of the six mice received an additional $70 \mu\text{g}$ of unlabeled DS-5573 (3 mg/kg). A biodistribution study was performed on day 3 after injection.

Statistical analysis

A paired t-test was used to determine significant differences between tissues (%ID/g) of ⁸⁹Zr-DS-5573a biodistribution results in MDA-MB-231 and CT26 tumor-bearing mice. An unpaired t-test (Mann-Whitney) was used to determine significant differences between tumor volumes in treated and untreated groups at each time point and to compare tissues (%ID/g) of ⁸⁹Zr-DS-5573a biodistribution results in treated and untreated groups at each time point. Data are presented as the average \pm SD, unless stated differently, and p-values of ≤ 0.05 were considered significant. All analyses were done using Graphpad Prism version 6.03.

Results

Conjugation, radiolabeling and quality assurance of ⁸⁹Zr-labeled DS-5573a

DS-5573a specifically binds to human B7-H3, but not to murine B7-H3, as shown by ELISA (Figure 1A-B). Chelation of DS-5573a was shown to be achieved without loss of structural integrity by SDS-PAGE analysis under reducing and non-reducing conditions (Figure S1A-B). Df-Bz-NCS-

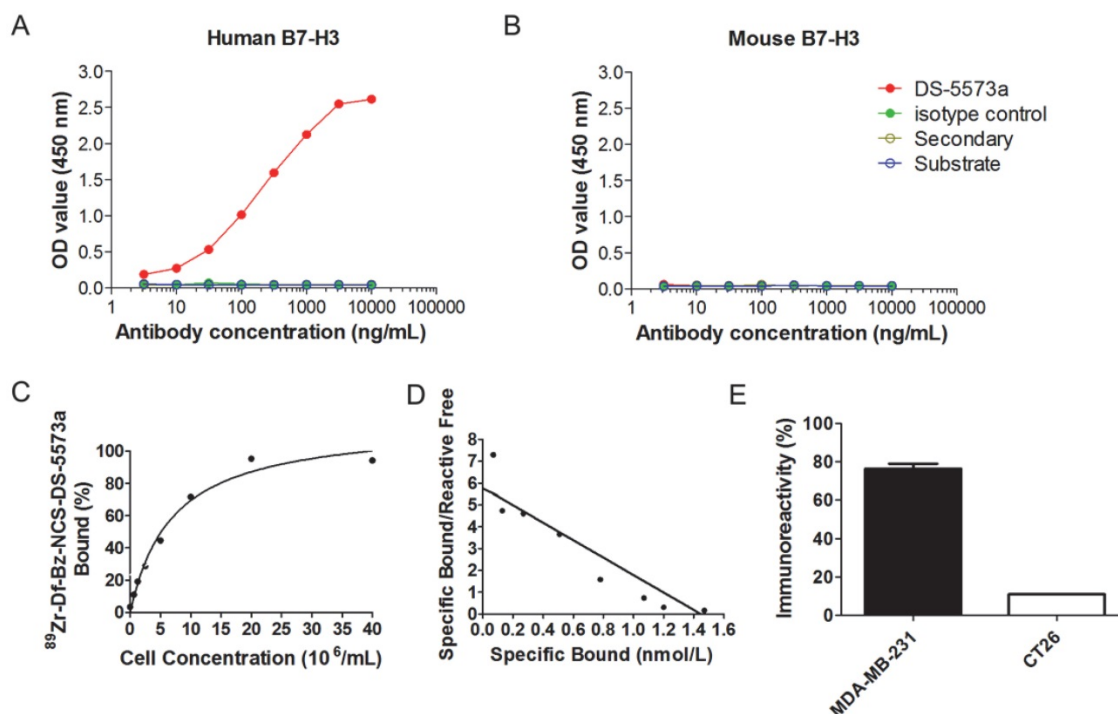


Figure 1. *In vitro* specific binding of DS-5573a and ⁸⁹Zr-Df-Bz-NCS-DS-5573a. (A) ELISA results showing specific binding of DS-5573a to human B7-H3. (B) ELISA results showing specific binding of DS-5573a to murine B7-H3. (C) Lindmo plot showing binding of ⁸⁹Zr-Df-Bz-NCS-DS-5573a to increasing concentrations of B7-H3-positive MDA-MB-231 cells. (D) Scatchard plot of ⁸⁹Zr-Df-Bz-NCS-DS-5573a to MDA-MB-231 cells. (E) Total binding of ⁸⁹Zr-Df-Bz-NCS-DS-5573a to 20×10^6 B7-H3-positive MDA-MB-231 versus B7-H3-negative CT26 cells ($n = 2$).

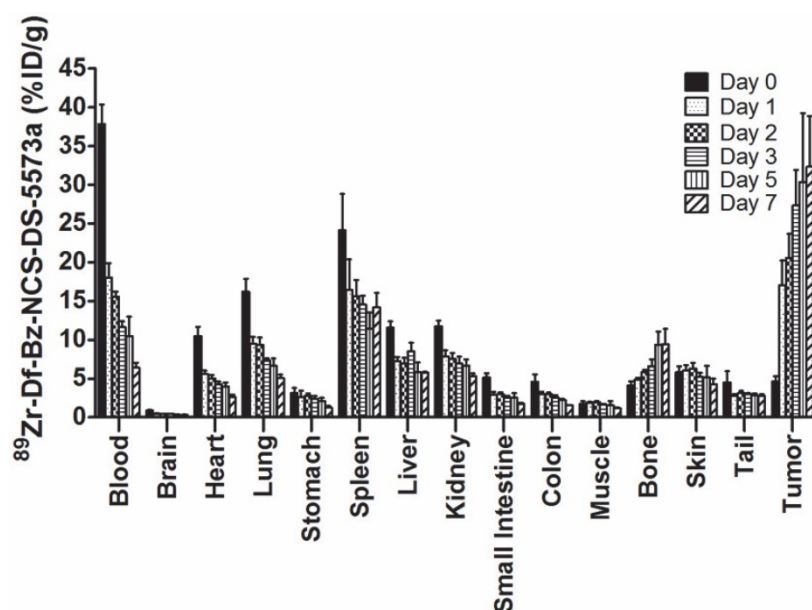


Figure 2. Biodistribution properties of ^{89}Zr -Df-Bz-NCS-DS-5573a in MDA-MB-231 xenograft BALB/c *nu/nu* mice over 7 days. Bars, mean \pm SD; $n = 5$.

DS-5573a was radiolabeled with ^{89}Zr at an efficiency of $88.9 \pm 2.8\%$ and high radiochemical purity ($99.3 \pm 0.2\%$). The immunoreactivity was $93.9 \pm 1.5\%$ (Figure 1C). Specific activity of ^{89}Zr -Df-Bz-NCS-DS-5573a was 86.95 ± 10.73 MBq/mg (2.35 ± 0.29 $\mu\text{Ci}/\mu\text{g}$) protein. Scatchard analysis indicated that the ^{89}Zr -conjugate had a K_a of $4.0 \times 10^9 \text{ M}^{-1}$ and the number of antibody binding sites per cell was 87,000 (Figure 1D). In a single-point binding assay, ^{89}Zr -DS-5573a showed high and specific binding to B7-H3-expressing MDA-MB-231 cells ($75.0 \pm 2.9\%$), and low binding to B7-H3-negative CT26 cells ($10.85 \pm 0.11\%$) (Figure 1E).

Stability data for ^{89}Zr -Df-DS-5573a after 7 days in human serum showed radiochemical purity remained high at 94.6% and immunoreactivity decreased to $57.2 \pm 2.0\%$. The integrity of the radioconjugate was maintained during the incubation period, as demonstrated by size exclusion chromatography analysis (Figure S1C-F).

Biodistribution studies and imaging with ^{89}Zr -labeled DS-5573a

Figure 2 summarizes the biodistribution results of ^{89}Zr -DS-5573a in B7-H3-positive MDA-MB-231 tumors in BALB/c *nu/nu* mice. ^{89}Zr -labeled DS-5573a demonstrated high tumor uptake, with normal tissues demonstrating clearance patterns typical of a radiolabeled intact humanized antibody. On day 0 (2 h post injection), the mean \pm SD levels of radioconjugate in tumor was 4.58 ± 0.69 %ID/g, increasing to 27.31 ± 4.61 %ID/g by day 3, which was maintained to day 7 with a value of 32.32 ± 6.55 %ID/g of tumor. There was some minor bone uptake, most likely due to localization of catabolized free ^{89}Zr .

The tumor-to-blood ratio increased from 0.12 ± 0.02 (day 0) to 5.03 ± 0.73 (day 7).

A higher dose of $66.5 \mu\text{Ci}$ of ^{89}Zr -Df-DS-5573a was administered to the mice for imaging studies. Whole-body PET/MR images confirmed excellent localization of ^{89}Zr -Df-DS-5573a to tumors established in the left flank on day 7 post injection (Figure 3). After imaging, mice were sacrificed and tumor uptake was compared at the different dose levels (i.e., $10.1 \mu\text{Ci}$ ($5 \mu\text{g}$) for biodistribution study versus $66.5 \mu\text{Ci}$ ($30 \mu\text{g}$) for imaging study). Comparable tumor uptake was seen at the two doses (biodistribution, 32.32 ± 7.32 %ID/g; imaging, 27.73 ± 3.30 %ID/g; $P = 0.42$).

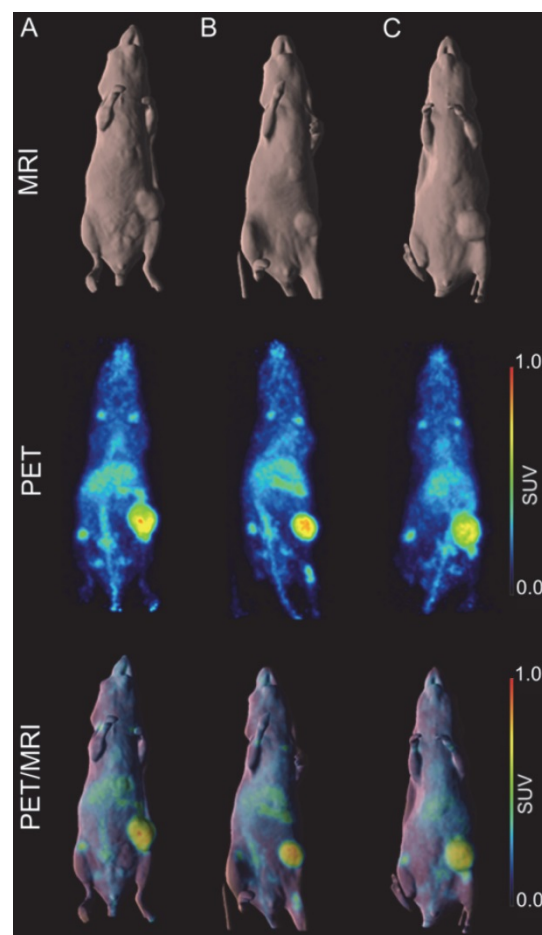


Figure 3. In vivo imaging of B7-H3 receptor in MDA-MB-231 tumor-bearing BALB/c *nu/nu* mice. (A) BALB/c *nu/nu* mouse bearing a MDA-MB-231 tumor of 322 mm^3 . (B) BALB/c *nu/nu* mouse bearing a MDA-MB-231 tumor of 240 mm^3 . (C) BALB/c *nu/nu* mouse bearing a MDA-MB-231 tumor of 393 mm^3 . MR (surface rendered, top row), PET (maximum intensity projection, middle row) and fused PET/MR (bottom row) images of each MDA-MB-231 xenograft mouse taken on day 7 post injection of ^{89}Zr -Df-Bz-NCS-DS-5573a.

Specific targeting of ^{89}Zr -labeled DS-5573a *in vivo*

SCID mice were selected for the remaining part of the study because the therapeutic activity of the DS-5573a antibody has previously been demonstrated in SCID mice [31]. Firstly, biodistribution of ^{89}Zr -DS-5573a (5 μg , 12.5 μCi) was compared in MDA-MB-231 tumor-bearing BALB/c *nu/nu* (313.4 \pm 51.8 mg, $n = 3$) and SCID (314.9 \pm 137.2 mg, $n = 3$) mice. In addition, to demonstrate specific targeting of DS-5573a *in vivo*, ^{89}Zr -DS-5573a was injected in human B7-H3-negative CT26 (512.5 \pm 218.6 mg, $n = 3$) tumor-bearing SCID mice. Biodistributions and PET/MR imaging were performed on day 3 post injection to keep tumor sizes comparable between each group.

Tumor uptake was significantly lower in B7-H3-negative CT26 tumors (10.07 \pm 0.79 %ID/g) compared to both MDA-MB-231 tumors in SCID (35.90 \pm 3.59 %ID/g, $P < 0.0005$) as well as MDA-MB-231 in BALB/c *nu/nu* mice (29.62 \pm 5.71.30 %ID/g, $P < 0.001$), demonstrating specific targeting of ^{89}Zr -DS-5573a *in vivo* (Figure 4). All other organs in the two strains did not show significant differences in ^{89}Zr -DS-5573a uptake, with the exception of the spleen. Significantly higher spleen uptake was observed in tumor-bearing SCID mice (MDA-MB-231, 28.95 \pm 1.65 %ID/g; CT26, 30.35 \pm 0.30 %ID/g) versus BALB/c *nu/nu* mice (MDA-MB-231, 14.80 \pm 0.50 %ID/g) ($P < 0.005$). The average spleen size of SCID mice (47.2 \pm 3.0 mg, $n = 30$) was significantly smaller than BALB/c *nu/nu* mice (91.5 \pm 2.6 mg, $n = 30$) (Figure S2A). Although comparable %ID ^{89}Zr -DS-5573a was measured in BALB/c *nu/nu* and SCID mice on day 3 (Figure S2D; BALB/c *nu/nu*, 1.47 \pm 0.28; SCID, 1.35 \pm 0.25) and day 7 (Figure S2E; BALB/c *nu/nu*, 1.36 \pm 0.25 %ID; SCID, 1.25 \pm 0.16 %ID), a significant difference in spleen size between the two strains on day 3 (BALB/c *nu/nu*, 0.101 \pm 0.014 g; SCID, 0.046 \pm 0.008 g; $P < 0.05$) and day 7 was measured (BALB/c *nu/nu*, 0.096 \pm 0.018; SCID, 0.059 \pm 0.003; $P < 0.05$) (Figure S2B-C) as well as a higher %ID/g of ^{89}Zr -DS-5573a in the spleens of tumor-bearing SCID mice versus BALB/c *nu/nu* mice on day 3 (BALB/c *nu/nu*, 14.53 \pm 1.33 %ID/g; SCID, 29.33 \pm 2.33 %ID/g; $P < 0.05$) and day 7 (BALB/c *nu/nu*, 14.17 \pm 2.06 %ID/g; SCID, 21.33 \pm 2.89 %ID/g; $P < 0.05$). This observation aligns with the differences in Fc-mediated uptake of IgG1 antibodies measured in non-targeted tissues of different mouse strains as shown recently by Sharma et al. [35]. Whole-body PET/MR images confirmed markedly reduced uptake of ^{89}Zr -DS-5573a in antigen-negative CT26 tumors versus antigen-positive MDA-MB-231 tumors in SCID mice on day 3 post injection (Figure 5).

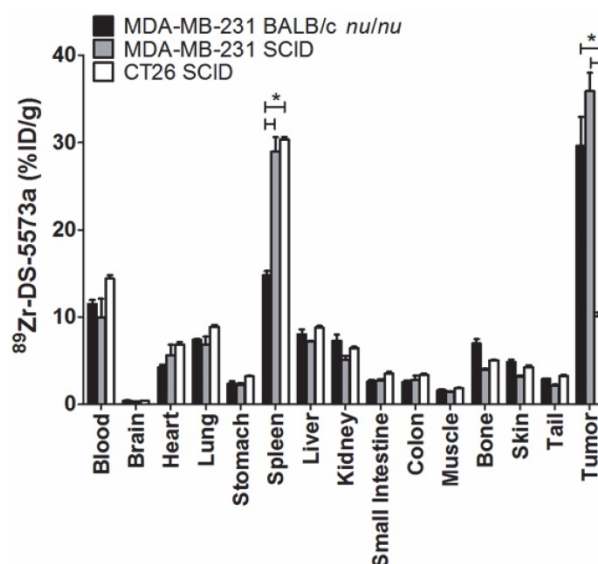


Figure 4. Specific targeting of ^{89}Zr -Df-Bz-NCS-DS-5573a *in vivo*. Biodistribution of ^{89}Zr -Df-Bz-NCS-DS-5573a in MDA-MB-231 tumor-bearing BALB/c *nu/nu* and SCID mice versus CT26 on day 3 post injection. Bars, mean \pm SEM; $n = 3$; *, $P \leq 0.05$.

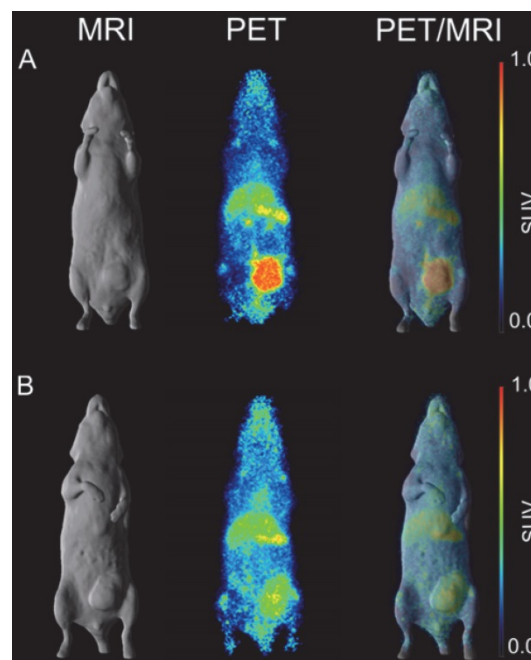


Figure 5. *In vivo* imaging of B7-H3 receptor in tumor-bearing SCID mice. (A) Representative whole-body surface-rendered MRI images (left column), maximum intensity projection PET images (middle column) and fused PET/MRI images (right column) of 5 μCi ^{89}Zr -Df-Bz-NCS-DS-5573a injected in a MDA-MB-231 tumor-bearing SCID mouse at day 3 post injection. (B) Representative whole-body surface-rendered MRI images (left column), maximum intensity projection PET images (middle column) and fused PET/MRI images (right column) of 5 μCi ^{89}Zr -Df-Bz-NCS-DS-5573a injected in a CT26 tumor-bearing SCID mouse at day 3 post injection.

Molecular imaging of B7-H3 with ^{89}Zr -labeled DS-5573a in combination with DS-5573a therapy

A combined imaging/therapy study was performed to demonstrate the theranostic potential of ^{89}Zr -DS-5573a. A schematic diagram of the set-up of

the experiment is shown in **Figure S3**. SCID mice with established MDA-MB-231 tumors ($83.37 \pm 13.13 \text{ mm}^3$, $n = 12$) were treated with DS-5573a (3 mg/kg in PBS) or vehicle control (PBS) at a weekly basis for four weeks in total (**Figure 6**, **Figure S3** and **Figure S4**). The percentage tumor growth inhibition (%TGI) after four weeks of therapy with DS-5573a was 89.8% (**Figure 6A-B**).

At commencement of therapy, a separate group of nine mice ($82.48 \pm 20.80 \text{ mm}^3$) was injected with ^{89}Zr -DS-5573a (5 μg , 0.02 mg/kg). Three out of nine mice received 5 μg labeled antibody (18.6 μCi), three out of nine received 5 μg labeled antibody (18.6 μCi) mixed with 70 μg of cold DS-5573a antibody to total a therapeutic dose of 3 mg/kg, and three out of nine mice received an imaging dose of 30 μg (112 μCi) with 45 μg of cold DS-5573a to total a therapeutic dose of 3 mg/kg. **Figure 6C** shows the results of the biodistribution study performed on day 3 post injection. Tumor uptake was significantly lower in the groups of mice receiving therapeutic doses of antibody (3 mg/kg), demonstrating saturation of the B7-H3 binding sites at that dose level (5 μg ^{89}Zr -DS-5573a, $58.98 \pm 16.86 \text{ \%ID/g}$; 5 μg ^{89}Zr -DS-5573a + 70 μg cold DS-5573a, $16.04 \pm 1.97 \text{ \%ID/g}$; 30 μg ^{89}Zr -DS-5573a + 45 μg cold DS-5573a, $17.90 \pm 3.13 \text{ \%ID/g}$).

All other organs did not show significant differences in ^{89}Zr -DS-5573a uptake, with the exception of the spleen. Significantly higher spleen uptake was observed in the 5 μg ^{89}Zr -DS-5573a group ($29.72 \pm 2.25 \text{ \%ID/g}$) and the 30 μg ^{89}Zr -DS-5573a + 45 μg cold DS-5573a group ($38.24 \pm 6.14 \text{ \%ID/g}$) versus the 5 μg ^{89}Zr -DS-5573a + 70 μg cold DS-5573a group ($18.39 \pm 4.07 \text{ \%ID/g}$). Again, the differences in spleen uptake were attributed to the differences in spleen sizes between groups and its effect on Fc-mediated uptake of DS-5573a antibody (spleen 5 μg ^{89}Zr -DS-5573a, $41 \pm 5 \text{ mg}$; spleen 5 μg ^{89}Zr -DS-5573a + 70 μg cold DS-5573a, $52 \pm 7 \text{ mg}$; spleen 30 μg ^{89}Zr -DS-5573a + 45 μg cold DS-5573a, $24 \pm 3 \text{ mg}$).

One week after the final administration of therapy of DS-5573a or vehicle control, a combination of a biodistribution and PET/MR imaging study was performed. In each therapy group ($n = 6$), three mice received 5 μg labeled antibody (13.3 μCi) and three mice received 5 μg labeled antibody (13.3 μCi) mixed with 70 μg of cold DS-5573a antibody to total a therapeutic dose of 3 mg/kg. On day 7 post injection, biodistribution was performed on all mice (**Figure 6D**). PET/MR imaging was performed on a representative mouse of each group on day 7 post injections (**Figure 6E**). Significantly reduced tumor uptake was observed in the treated group (Tx) versus the vehicle control group (PBS) injected with tracer

dose of 5 μg ^{89}Zr -DS-5573a (Tx = $16.17 \pm 2.14 \text{ \%ID/g}$ PBS = $25.76 \pm 1.80 \text{ \%ID/g}$; $P < 0.001$). Blocking of binding sites was demonstrated by comparing tumor uptake in mice receiving a tracer dose of 5 μg ^{89}Zr -DS-5573a with tumor uptake in mice receiving a blocking dose of 5 μg ^{89}Zr -DS-5573a mixed with 70 μg cold DS-5573a. Tumor uptake was reduced from $25.76 \pm 1.80 \text{ \%ID/g}$ to $12.48 \pm 1.35 \text{ \%ID/g}$ in the vehicle control group and from $25.76 \pm 1.80 \text{ \%ID/g}$ to $13.24 \pm 1.35 \text{ \%ID/g}$ in the DS-5573a-treated group (**Figure 6D-E**). This indicates that even one week after final therapy injection, the binding sites in the MDA-MB-231 tumors of DS-5573a-treated mice remain blocked, suggesting that a weekly injection of DS-5573a suffices to keep the B7-H3 receptors blocked.

Biodistribution results on day 7 post injection show that the majority of organs of the DS-5573a treated mice (blood, heart, lung, stomach, kidneys, small intestine, colon, bone, skin and tail) show a significant increase in \%ID/g compared to the organs of the vehicle control groups (**Figure 6D**). The increased activity in these organs suggests a delay in antibody clearance in treated mice compared to vehicle control mice due to the weekly injections of 3 mg/kg DS-5573a. In contrast, spleen uptake is reduced in the treated mice versus untreated mice, which can also be explained by the delayed blood clearance and catabolism of ^{89}Zr -DS-5573a in the presence of increased blood levels of cold DS-5573a.

Discussion

Immunotherapy drugs are being evaluated in essentially all tumor types and some, targeting CLTA or PD-1, have already entered standard medical practice [36-39]. However, there remain significant challenges ahead, including optimising patient selection and understanding mechanisms of resistance. Development of new drugs is therefore important; amongst these, are drugs targeting the B7-H3 family.

A number of monoclonal antibodies targeting B7-H3 have been tested in preclinical models [40, 41]. Enoblituzumab (MGA271) is a humanised IgG1 monoclonal antibody engineered to potentiate antibody-dependent cell-mediated cytotoxicity [28]. Interim results from a phase 1 dose escalation study (National Clinical Trial (NCT) 01391143) evaluating MGA271 in a variety of high-B7-H3-expressing tumors shows a favourable safety profile with early evidence of efficacy [42]. A two-component cohort expansion (NCT01391143) is underway. MGA271 is also being evaluated in combination with ipilimumab (NCT02381314) and pembrolizumab (NCT02475213) in early phase clinical trials. 8H9 is a humanised IgG1

monoclonal antibody targeting B7-H3 [43]. 8H9 radiolabeled with ¹³¹I and ¹²⁴I is being evaluated in

CNS tumors (NCT01502917 and NCT00089245) and peritoneal metastases (NCT01099644).

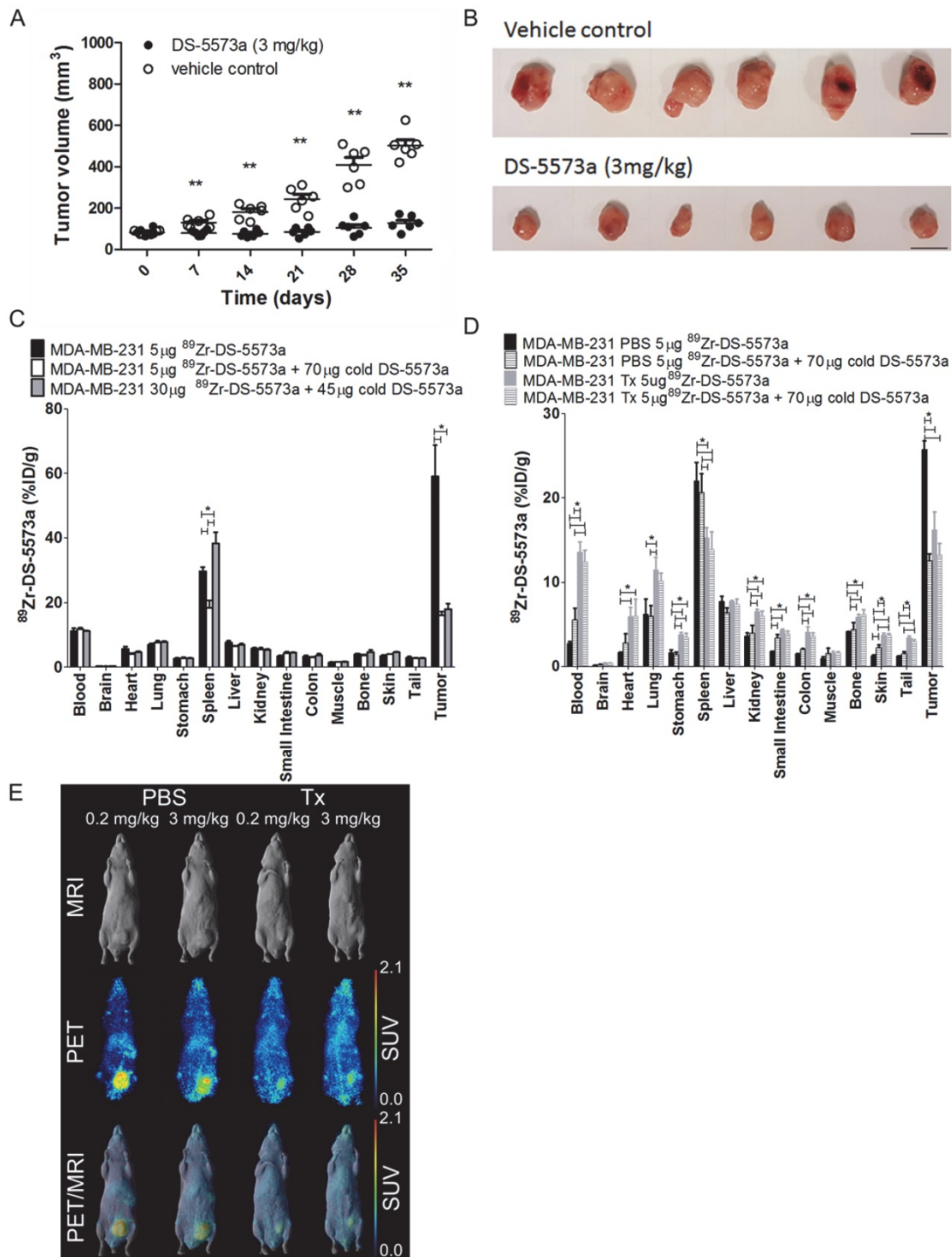


Figure 6. Theranostic properties of ⁸⁹Zr-DS-5573a in MDA-MB-231 tumor-bearing SCID mice treated weekly with 3 mg/kg DS-5573 or vehicle control for a total of four weeks. (A) Tumor volumes measured with a caliper in DS-5573a-treated and vehicle control mice (n = 6). (B) Tumors removed from DS-5573a-treated (lower panel) and vehicle control (upper panel) mice at 35 days post treatment. Scale bar, 1 cm. (C) Specific targeting of ⁸⁹Zr-Df-Bz-NCS-DS-5573a in vivo demonstrated at the start of therapy. Biodistribution of different concentrations of ⁸⁹Zr-Df-Bz-NCS-DS-5573a in MDA-MB-231 tumor-bearing SCID mice on day 3 post injection (n = 3). (D) Specific targeting of ⁸⁹Zr-Df-Bz-NCS-DS-5573a in vivo demonstrated at the end of therapy. Biodistribution of ⁸⁹Zr-Df-Bz-NCS-DS-5573a in MDA-MB-231 tumor-bearing SCID mice treated for four weeks with 3 mg/kg DS-5573a (Tx, n = 6) or vehicle control (PBS, n = 6) on day 7 post injection. One week after the final treatment, half of each therapy group was injected with 5 μg ⁸⁹Zr-Df-Bz-NCS-DS-5573a and the other half was injected with 5 μg ⁸⁹Zr-Df-Bz-NCS-DS-5573a mixed with 70 μg cold DS-5573a (3 mg/kg). (E) In vivo saturation of B7-H3 at a therapeutic dose level of 3 mg/kg DS-5573a demonstrated by PET/MRI. Representative whole-body surface-rendered MRI images (top row), maximum intensity projection PET images (middle row) and fused PET/MRI images (bottom row) are shown on day 7 post injection of ⁸⁹Zr-Df-Bz-NCS-DS-5573a in vehicle control-treated mice (PBS) and DS-5573a-treated (3 mg/kg) mice (Tx). To demonstrate specific binding in each therapy group, mice were injected with 5 μg ⁸⁹Zr-Df-Bz-NCS-DS-5573a (0.2 mg/kg) or 5 μg ⁸⁹Zr-Df-Bz-NCS-DS-5573a mixed with 70 μg cold DS-5573a (3 mg/kg). The hot spot visible in PET and PET/MRI images of the PBS-treated mouse receiving 3 mg/kg is due to a blood crust (Figure S4). Bars, mean ± SEM; *, P ≤ 0.05; **, P ≤ 0.01.

In this study, we report on the successful radiolabeling of DS-5573a and explore the potential theranostic use of ^{89}Zr -Df-Bz-NCS-DS-5573a as an imaging probe in combination with unlabeled DS-5573a targeting B7-H3-expressing tumors. Preclinical studies show DS-5573a has potent antitumor activity mediated by antibody-dependent cellular cytotoxicity and phagocytosis [31]. We report the first imaging of B7-H3 expression on cancer cells using ^{89}Zr with a PET imaging approach showing excellent resolution and ability to quantify tumor uptake. The study demonstrated the specific targeting of ^{89}Zr -Df-Bz-NCS-DS-5573a in B7-H3-expressing tumors, *in vitro* as well as *in vivo* using PET molecular imaging of B7-H3 expression on tumor cells. ^{89}Zr -Df-Bz-NCS-DS-5573a was stable in serum at 37 °C with retention of immunoreactivity, radiochemical purity and construct integrity for up to 7 days. The biodistribution study demonstrated high uptake of ^{89}Zr -Df-Bz-NCS-DS-5573a in tumors, with levels rising by day 3 and maintained to day 7. The stable *in vivo* properties of ^{89}Zr -Df-Bz-NCS-DS-5573a were comparable to previously reported IgG1 humanized antibodies [32, 44, 45]. Uptake of ^{89}Zr -Df-Bz-NCS-DS-5573a was higher in the spleen of SCID mice versus BALB/c *nu/nu* mice. A smaller spleen size was measured in SCID mice versus BALB/c *nu/nu* mice, which can contribute to an increased uptake in the spleen of SCID mice. A similar observation has been made by England *et al.* in immunodeficient NSG mice [46]. Furthermore, a recent publication by Sharma *et al.* demonstrated that the immunodeficiency status of the mouse host as well as both the biological origin and glycosylation of the antibody contribute significantly to differences in the biodistribution of therapeutic monoclonal antibodies [35]. As shown by Sharma *et al.*, the interaction between Fc gamma receptors (F γ Rs) expressed by immune effector cells of myeloid origin (such as monocytes/macrophages prevalent in the spleen and a subset of dendritic cells and neutrophils in the bone marrow) and the Fc portion of antibodies results in anomalous biodistribution of radioimmunoconjugates in non-target organs such as the spleen of mice that have a highly immunodeficient background. Furthermore, the glycosylation status of the DS-5573a, an afucosylated human IgG1 antibody with increased binding affinity for Fc γ RIIIa, could have contributed to the non-target uptake of ^{89}Zr -DS-5573a in organs such as bone and spleen when compared to previously reported ^{89}Zr -labeled humanized IgG1 antibodies [32, 35, 44, 45].

A higher imaging dose of 66.5 μCi (30 μg) of ^{89}Zr -Df-Bz-NCS-DS-5573a was initially administered to the MDA-MB-231 BALB/c *nu/nu* mice for

PET/MRI imaging. Comparable tumor uptake was seen between the 30 μg imaging dose level and the 5 μg biodistribution dose level (biodistribution, 32.32 ± 7.32 %ID/g; imaging, 27.73 ± 3.30 %ID/g; $P = 0.42$). In contrast, a biodistribution study in MDA-MB-231 tumor-bearing SCID mice showed that at a therapeutic dose of 3 mg/kg (i.e., 30 μg mixed with 45 μg cold DS-5573a), saturation occurs. These results show the ability of ^{89}Zr -Df-Bz-NCS-DS-5573a to measure receptor occupancy *in vivo*, and that receptor saturation can be observed at doses required for therapeutic effects.

A murine colon cancer cell line CT26 was used as a negative control. We demonstrated that DS-5573a does not bind the murine B7-H3, and therefore, the use of this model was justified as no therapeutic activity of DS-5573a in CT26 tumors is expected. However, the absence of human B7-H3 in normal mouse tissue does not reflect normal B7-H3 expression in normal human tissues and a clinical trial study with ^{89}Zr -Df-Bz-NCS-DS-5573a is needed to show normal B7-H3 expression and related ^{89}Zr -Df-Bz-NCS-DS-5573a uptake.

The impact of therapeutic activity of DS-5573a on ^{89}Zr -Df-Bz-NCS-DS-5573a biodistribution and tumor uptake was investigated in a combined imaging/therapy study. Both biodistribution and PET/MR imaging demonstrated reduced tumor uptake of trace radiolabeled ^{89}Zr -Df-Bz-NCS-DS-5573a (0.2 mg/kg) in the presence of 3 mg/kg therapeutic dose of DS-5573a. Comparison of the uptake of ^{89}Zr -Df-Bz-NCS-DS-5573a (0.2 mg/kg) in antigen-negative CT26 tumors versus uptake of ^{89}Zr -DS-5573a at different dose levels (0.2 mg/kg versus 3 mg/kg) shows that saturation occurs in DS-5573a-treated mice, and that the tumors remain saturated for at least one week after four weeks of therapy. This offers the opportunity in a clinical setting to measure saturation of B7-H3 in patients.

A full comparison on the effect on biodistribution of B7-H3 acting as a sink was not investigated. However, on day 3 post injection the difference in blood activity when comparing blood from MDA-MB-231 tumor-bearing mice versus CT26 tumor-bearing mice, can provide indirect evidence. Blood activity in CT26 tumor-bearing mice was 14.41 ± 0.72 %ID/g versus 9.96 ± 3.72 %ID/g in MDA-MB-231 tumor-bearing SCID mice. This difference suggests there might be a small effect on biodistribution of B7-H3 acting as a sink.

The ability to use ^{89}Zr -Df-Bz-NCS-DS-5573a as molecular imaging probe for patients undergoing immunotherapy treatment is part of a crucial effort to enable patient selection and understand the biology of these drugs better. As immune-modulatory drugs

become standard of care, evaluating tumor responses can be challenging especially when attempting to differentiate metabolically active cancer cells from activated immune cells. Multiple molecular imaging techniques using emission tomography have been evaluated, including direct *ex vivo* labeling of T lymphocytes with radioactive probes [47, 48], indirect labeling of immune cells *in vivo* using PET reporter gene expression [49, 50], small-molecule PET tracers and radiolabeled intact antibodies. High PD-L1 expression has been shown to correlate with anti-tumor response of anti-PD-1 therapy [51]. B7-H3 overexpression is associated with a poor outcome; however, its effect on anti-tumor activity of immunotherapies remains unknown. ^{89}Zr -Df-Bz-NCS-DS-5573a has the potential to be an ideal PET tracer by providing real-time quantitation, and detection of heterogeneity and dynamic changes in B7-H3 expression, all of which can be useful for guiding and monitoring therapy responses and therefore select patients most likely to benefit from immunotherapy. Furthermore, ^{89}Zr -DS-5573a binds to B7-H3, which is typically only expressed in cancer cells and therefore binding is not proliferation-dependent.

In conclusion, this study has demonstrated specific and prolonged targeting of ^{89}Zr -Df-Bz-NCS-DS-5573a in B7-H3-expressing xenografts. Therefore, ^{89}Zr -Df-Bz-NCS-DS-5573a has the potential to quantify non-invasively B7-H3 target expression of tumors in cancer patients, as well as aid with dose selection in human phase 1 clinical studies.

Abbreviations

B7-H3: B7 homolog 3 or CD276; C: mean tumor volume of control at endpoint; C_0 : mean tumor volume of vehicle control at time 0; Df-Bz-NCS: *p*-isothiocyanatobenzyl-desferrioxamine; ITLC: instant thin layer chromatography; MRI: magnetic resonance imaging; NCT: National Clinical Trial; PBS: phosphate-buffered saline; PET: positron emission tomography; SEC: size exclusion chromatography; T_0 : mean tumor volume of treated at endpoint; T_0 : mean tumor volume of treated at time 0; %TGI: percentage tumor growth inhibition; Tx: treated group.

Supplementary Material

Supplementary figures.

<http://www.thno.org/v08p4199s1.pdf>

Acknowledgements

This work was supported by funding from Daiichi-Sankyo Co., Ltd. We acknowledge the Australian Cancer Research Foundation for providing funds to purchase the PET/MRI and nanoSPECT/CT

imaging equipment. This research was also undertaken using the Solid Target Laboratory, an ANSTO-Austin-LICR Partnership. The support of the Operational Infrastructure Support Program of the Victorian State Government; SP (LaTrobe University PhD Scholarship) and AMS (NHRMC Practitioner Fellowship APP1084178) is acknowledged.

Competing interests

Masakatsu Kotsuma, Kenji Hirotani and Giorgio Senaldi are employees of Daiichi Sankyo Co. Ltd. This work was supported by funding from Daiichi Sankyo Co. Ltd.

References

- Zang X, Loke Pn, Kim J, Murphy K, Waitz R, Allison JP. B7x: a widely expressed B7 family member that inhibits T cell activation. *Proc Natl Acad Sci USA*. 2003; 100: 10388-92.
- Spira AI, Park K, Mazieres J, Vansteenkiste JF, Rittmeyer A, Ballinger M, et al. Efficacy, safety and predictive biomarker results from a randomized phase II study comparing MPDL3280A vs docetaxel in 2L/3L NSCLC (POPLAR). *J Clin Oncol*. 2015; 33 (Suppl 15): 8010.
- Rizvi NA, Brahmer JR, Ou S-HI, Segal NH, Khleif S, Hwu W-J, et al. Safety and clinical activity of MEDI4736, an anti-programmed cell death-ligand 1 (PD-L1) antibody, in patients with non-small cell lung cancer (NSCLC). *J Clin Oncol*. 2015; 33 (Suppl 15): 8032.
- Disis ML, Patel MR, Pant S, Infante JR, Lockhart AC, Kelly K, et al. Avelumab (MSB0010718C), an anti-PD-L1 antibody, in patients with previously treated, recurrent or refractory ovarian cancer: A phase Ib, open-label expansion trial. *J Clin Oncol*. 2015; 33 (Suppl 15): 5509.
- Apolo AA, Infante JR, Balmanoukian A, Patel MR, Wang D, Kelly K, et al. Avelumab, an anti-programmed death-ligand 1 antibody, in patients with refractory metastatic urothelial carcinoma: Results from a multicenter, phase Ib study. *J Clin Oncol*. 2017; 35: 2117-24.
- Fehrenbacher L, Spira A, Ballinger M, Kowanzet M, Vansteenkiste J, Mazieres J, et al. Atezolizumab versus docetaxel for patients with previously treated non-small-cell lung cancer (POPLAR): a multicentre, open-label, phase 2 randomised controlled trial. *Lancet*. 2016; 387: 1837-46.
- Rosenberg JE, Hoffman-Censits J, Powles T, van der Heijden MS, Balar AV, Necchi A, et al. Atezolizumab in patients with locally advanced and metastatic urothelial carcinoma who have progressed following treatment with platinum-based chemotherapy: a single-arm, multicentre, phase 2 trial. *Lancet*. 2016; 387: 1909-20.
- Sun M, Richards S, Prasad DV, Mai XM, Rudensky A, Dong C. Characterization of mouse and human B7-H3 genes. *J Immunol*. 2002; 168: 6294-7.
- Chapoval AI, Ni J, Lau JS, Wilcox RA, Flies DB, Liu D, et al. B7-H3: a costimulatory molecule for T cell activation and IFN- γ production. *Nat Immunol*. 2001; 2: 269-74.
- Prasad DV, Nguyen T, Li Z, Yang Y, Duong J, Wang Y, et al. Murine B7-H3 is a negative regulator of T cells. *J Immunol*. 2004; 173: 2500-6.
- Leitner J, Klausner C, Pickl WF, Stöckl J, Majdic O, Bardet AF, et al. B7-H3 is a potent inhibitor of human T-cell activation: No evidence for B7-H3 and TREM2 interaction. *Eur J Immunol*. 2009; 39: 1754-64.
- Castriconi R, Dondero A, Augugliaro R, Cantoni C, Carnemolla B, Sementa AR, et al. Identification of 4g-B7-H3 as a neuroblastoma-associated molecule that exerts a protective role from an NK cell-mediated lysis. *Proc Natl Acad Sci USA*. 2004; 101: 12640-5.
- Loos M, Hedderich DM, Friess H, Kleeff J. B7-H3 and its role in antitumor immunity. *Clin Dev Immunol*. 2010; 2010: 683875.
- Sun J, Chen LJ, Zhang GB, Jiang JI, Zhu M, Tan Y, et al. Clinical significance and regulation of the costimulatory molecule B7-H3 in human colorectal carcinoma. *Cancer Immunol Immun*. 2010; 59: 1163-71.
- Kang FB, Wang L, Jia HC, Li D, Li HJ, Zhang YG, et al. B7-H3 promotes aggression and invasion of hepatocellular carcinoma by targeting epithelial-to-mesenchymal transition via JAK2/STAT3/Slug signaling pathway. *Cancer Cell Int*. 2015; 15: 45.
- Xu H, Cheung Y, Guo HF, Cheung NKV. MicroRNA miR-29 modulates expression of immunoinhibitory molecule B7-H3: Potential implications for immune based therapy of human solid tumors. *Cancer Res*. 2009; 69: 6275-81.
- Bachawal SV, Jensen KC, Wilson KE, Tian L, Lutz AM, Willmann JK. Breast cancer detection by B7-H3-targeted ultrasound molecular imaging. *Cancer Res*. 2015; 75: 2501-9.
- Sun J, Guo YD, Li XN, Zhang YQ, Gu L, Wu PP, et al. B7-H3 expression in breast cancer and upregulation of VEGF through gene silence. *Oncol Targets Ther*. 2014; 7: 1979-86.

19. Roth TJ, Sheinin Y, Lohse CM, Kuntz SM, Frigola X, Inman BA, et al. B7-H3 ligand expression by prostate cancer: a novel marker of prognosis and potential target for therapy. *Cancer Res.* 2007; 67: 7893-900.
20. Zang X, Thompson RH, Al-Ahmadie HA, Serio AM, Reuter VE, Eastham JA, et al. B7-H3 and B7x are highly expressed in human prostate cancer and associated with disease spread and poor outcome. *Proc Natl Acad Sci USA.* 2007; 104: 19458-63.
21. Zang X, Sullivan PS, Soslow RA, Waitz R, Reuter VE, Wilton A, et al. Tumor associated endothelial expression of B7-H3 predicts survival in ovarian carcinomas. *Mod Pathol.* 2010; 23: 1104-12.
22. Crispin PL, Sheinin Y, Roth TJ, Lohse CM, Kuntz SM, Frigola X, et al. Tumor cell and tumor vasculature expression of B7-H3 predict survival in clear cell renal cell carcinoma. *Clin Cancer Res.* 2008; 14: 5150-7.
23. Ingebrigtsen VA, Boye K, Nesland JM, Nesbakken A, Flatmark K, Fodstad Ø. B7-H3 expression in colorectal cancer: associations with clinicopathological parameters and patient outcome. *BMC cancer.* 2014; 14: 602.
24. Boorjian SA, Sheinin Y, Crispin PL, Farmer SA, Lohse CM, Kuntz SM, et al. T-cell coregulatory molecule expression in urothelial cell carcinoma: clinicopathologic correlations and association with survival. *Clin Cancer Res.* 2008; 14: 4800-8.
25. Kraan J, van den Broek P, Verhoef C, Grunhagen D, Taal W, Gratama J-W, et al. Endothelial CD276 (B7-H3) expression is increased in human malignancies and distinguishes between normal and tumour-derived circulating endothelial cells. *Br J Cancer.* 2014; 111: 149-56.
26. Chen Y-W, Tekle C, Fodstad O. The immunoregulatory protein human B7H3 is a tumor-associated antigen that regulates tumor cell migration and invasion. *Curr Cancer Drug Targets.* 2008; 8: 404-13.
27. Yuan H, Wei X, Zhang G, Li C, Zhang X, Hou J. B7-H3 over expression in prostate cancer promotes tumor cell progression. *J Urol.* 2011; 186: 1093-9.
28. Loo D, Alderson RF, Chen FZ, Huang L, Zhang W, Gorlatov S, et al. Development of an Fc-enhanced anti-B7-H3 monoclonal antibody with potent antitumor activity. *Clin Cancer Res.* 2012; 18: 3834-45.
29. Zang X, Allison JP. The B7 family and cancer therapy: costimulation and coinhibition. *Clin Cancer Res.* 2007; 13: 5271-9.
30. Xie C, Liu D, Chen Q, Yang C, Wang B, Wu H. Soluble B7-H3 promotes the invasion and metastasis of pancreatic carcinoma cells through the TLR4/NF-κB pathway. *Sci Rep.* 2016; 6: 27528.
31. Nagase-Zembutsu A, Hirotani K, Yamato M, Yamaguchi J, Takata T, Yoshida M, et al. Development of DS-5573a: A novel afucosylated monoclonal antibody directed at B7-H3 with potent antitumor activity. *Cancer Sci.* 2016; 107: 674-81.
32. Burvenich IJ, Parakh S, Gan HK, Lee F-T, Guo N, Rigopoulos A, et al. Molecular imaging and quantitation of EphA2 expression in xenograft models with 89Zr-DS-8895a. *J Nucl Med.* 2016; 57: 974-80.
33. Lindmo T, Boven E, Cuttitta F, Fedorko J, Bunn P. Determination of the immunoreactive function of radiolabeled monoclonal antibodies by linear extrapolation to binding at infinite antigen excess. *J Immunol Methods.* 1984; 72: 77-89.
34. Lee FT, Rigopoulos A, Hall C, Clarke K, Cody SH, Smyth FE, et al. Specific localization, gamma camera imaging, and intracellular trafficking of radiolabelled chimeric anti-G(D3) ganglioside monoclonal antibody KM871 in SK-MEL-28 melanoma xenografts. *Cancer Res.* 2001; 61: 4474-82.
35. Sharma SK, Chow A, Monette S, Vivier D, Pourat J, Edwards KJ, et al. Fc-mediated anomalous biodistribution of therapeutic antibodies in immunodeficient mouse models. *Cancer Res.* 2018; 78: 1820-32.
36. Robert C, Schachter J, Long GV, Arance A, Grob JJ, Mortier L, et al. Pembrolizumab versus ipilimumab in advanced melanoma. *N Engl J Med.* 2015; 372: 2521-32.
37. Robert C, Long GV, Brady B, Dutriaux C, Maio M, Mortier L, et al. Nivolumab in previously untreated melanoma without BRAF mutation. *N Engl J Med.* 2015; 372: 320-30.
38. Brahmer J, Reckamp KL, Baas P, Crinò L, Eberhardt WE, Poddubska E, et al. Nivolumab versus docetaxel in advanced squamous-cell non-small-cell lung cancer. *N Engl J Med.* 2015; 373: 123-35.
39. Herbst RS, Baas P, Kim DW, Felip E, Pérez-Gracia JL, Han JY, et al. Pembrolizumab versus docetaxel for previously treated, PD-L1-positive, advanced non-small-cell lung cancer (KEYNOTE-010): a randomised controlled trial. *Lancet.* 2016; 387: 1540-50.
40. Fauci JM, Sabbatino F, Wang Y, Londoño-Joshi AI, Straughn JM, Landen CN, et al. Monoclonal antibody-based immunotherapy of ovarian cancer: Targeting ovarian cancer cells with the B7-H3-specific mAb 376.96. *Gynecol Oncol.* 2014; 132: 203-10.
41. Liang TW, Roberts PE, Young P, Li P, Santos MA, Chen F, et al. TES7, a monoclonal antibody targeting B7-H3, potently inhibits Hs-700T growth in vivo. *FASEB J.* 2008; 22 (Suppl 1): 321.11.
42. Powderly J, Cote G, Flaherty K, Szmulewitz RZ, Ribas A, Weber J, et al. Interim results of an ongoing Phase I, dose escalation study of MGA271 (Fc-optimized humanized anti-B7-H3 monoclonal antibody) in patients with refractory B7-H3-expressing neoplasms or neoplasms whose vasculature expresses B7-H3. *J Immunother Cancer.* 2015; 3 (Suppl 2): O8.
43. Ahmed M, Cheng M, Zhao Q, Goldgur Y, Cheal SM, Guo H-F, et al. Humanized affinity-matured monoclonal antibody 8H9 has potent antitumor activity and binds to FG loop of tumor antigen B7-H3. *J Biol Chem.* 2015; 290: 30018-29.
44. Holland JP, Divilov V, Bander NH, Smith-Jones PM, Larson SM, Lewis JS. 89Zr-DFO-J591 for immunoPET of prostate-specific membrane antigen expression in vivo. *J Nucl Med.* 2010; 51: 1293-300.
45. Dijkers EC, Kosterink JG, Rademaker AP, Perk LR, van Dongen GA, Bart J, et al. Development and characterization of clinical-grade 89Zr-trastuzumab for HER2/neu immunoPET imaging. *J Nucl Med.* 2009; 50: 974-81.
46. England CG, Jiang D, Eherding EB, Rekoske BT, Ellison PA, Hernandez R, et al. (89)Zr-labeled nivolumab for imaging of T-cell infiltration in a humanized murine model of lung cancer. *Eur J Nucl Med Mol Imaging.* 2018; 45: 110-20.
47. Adonai N, Nguyen KN, Walsh J, Iyer M, Toyokuni T, Phelps ME, et al. Ex vivo cell labeling with 64Cu-pyruvaldehyde-bis (N4-methylthiosemicarbazone) for imaging cell trafficking in mice with positron-emission tomography. *Proc Natl Acad Sci USA.* 2002; 99: 3030-5.
48. Botti C, Negri DR, Seregini E, Ramakrishna V, Arienti F, Maffioli L, et al. Comparison of three different methods for radiolabelling human activated T lymphocytes. *Eur J Nucl Med.* 1997; 24: 497-504.
49. Herschman HR. Noninvasive imaging of reporter gene expression in living subjects. *Adv Cancer Res.* 2004; 92: 29-80.
50. Herschman HR. PET reporter genes for noninvasive imaging of gene therapy, cell tracking and transgenic analysis. *Crit Rev Oncol Hematol.* 2004; 51: 191-204.
51. Gandini S, Massi D, Mandala M. PD-L1 expression in cancer patients receiving anti PD-1/PD-L1 antibodies: A systematic review and meta-analysis. *Crit Rev Oncol Hematol.* 2016; 100: 88-98.